Progress In Electromagnetics Research C, Vol. 104, 53–67, 2020

A Compact Quad-Port Band-Notched MIMO Antenna for Wi-MAX Application with Low Mutual Coupling

Bhakti V. Nikam* and Maruti R. Jadhav

Abstract—High data rates and good channel bandwidth are some of the requirements of today's wireless communication systems. The wireless communication systems are now rapidly adopting a Multiple Input Multiple Output, i.e., MIMO technique due to its advantages such as the data rates and bandwidth. The main focus of this paper is to design a highly isolated MIMO antenna with Wi-MAX bandwidth. This MIMO antenna design is prepared with four pentagonal slotted monopole antennas with a parasitic element structure operating in the band of 5.1 to 5.8 GHz which offers isolation more than 28 dB. Rectangular slots are used for each radiating patch for a band-notched frequency at 5.5 GHz frequency relative to the Wi-MAX frequency band. To improve the isolation of the antenna, on the surface of the dielectric substrate, a single plus-shaped parasitic structure is uniformly inserted between the antenna elements. The result obtained from the fabricated antenna is at an acceptable range with that of the simulated for the Wi-MAX band applications.

1. INTRODUCTION

The extraordinary advances in wireless technologies led to the raised requests for higher information rates and a higher limit in wireless applications, for example, Wi-Fi, Bluetooth, WLAN, LTE, and Wi-MAX. MIMO system lies in various antennas at the receiving and transmitting sides, which gives promising ways to deal with the requirements of higher information rates without having additional influence in rich dissipating conditions [1]. They are fitted intently together on typical substrates. While accomplishing the best execution of the system, the isolation between the antenna components in MIMO must be as high as could be expected under various circumstances. The MIMO technology has been considered as an essential requirement for rising and future wireless communication benchmarks including Long term Evolution (4G), HSPA+ (3G), IEEE 802.11n (Wi-Fi), Wi-MAX (4G), and IEEE 802.11ac (Wi-Fi) [2]. The high isolation effect can be achieved by using two parasitic elements inserted in the ground plane for the UWB MIMO antenna with an active band in 3.3 to 3.8 GHz utilizing L- and U-shaped slots [3]. The band-notched reconfigurable signal in a MIMO configuration is made by attaching the PIN diodes and Ω-formed open structure to the system radiators. The notch is indicated by the frequency of the Wi-MAX facility at 3.5 GHz in the range of 3.2 to 3.8 GHz by changing the PIN diode to 'ON' status [4]. The interdigital system is adopted for GSM, 4G LTE, and Wi-MAX applications. The interdigital capacitor method can control the subsequent harmonics as wanted and decrease the size of the antenna [5]. To eliminate unwanted interactions between the antenna elements, a decoupling structure is placed behind the substrate [6]. A T-shaped ground slot is introduced directly to provide better separation between the two ports. A parasitic structure is then introduced to the ground plane so that the notched frequency is not captured in the WLAN band [7]. A slot resonator coupling is presented [8] to minimize unwanted interactions between antenna elements. In [9], parasitic

Received 6 June 2020, Accepted 7 July 2020, Scheduled 23 July 2020
* Corresponding author: Bhakti V. Nikam (bhaktinikam111@gmail.com).
The authors are with the Department of Electronics and Telecommunication Engineering, Rajarambapu Institute of Technology, Islampur, India.

strips are introduced and designed to diminish the mutual coupling effect to 5.2 and 5.8 GHz range reported. An arrangement of slotted and parasitic structures is anticipated to get better isolation of the system [10]. Over the most recent couple of years, different advancements have been talked about to plan a MIMO antenna with high isolation. Utilizing a neutralization line, defected ground structure, metamaterial, and decoupling network has adequately improved the isolation capability. Until now, a few investigations have planned different band-notched UWB-MIMO antenna systems [11–22]. The MIMO antennas in [11–20] have a single notch band of 5.5 GHz. The dual notched band was acknowledged in [21], and a simple slot and a modified Y-shaped stub both helped increase isolation capability. An elliptically shaped ring led to 3.5 and 5.5 GHz which means double notched operating bands. In [22], a CSRR slot structure was embedded to each radiator to get the notched result at 3.5 and 5.5 GHz of the active band, while 8 GHz undesirable band was acknowledged by putting two C-shaped stubs evenly alongside the feed lines. While dual monopole components are put oppositely, the low coupling of 20 dB was achieved.

In this work, a compact quad element antenna is implemented and analyzed for four identical components with band-notched characteristics in the Wi-MAX frequency band. The antenna consists of four identical pentagonal radiators in the 5.1 to 5.8 GHz band and a notched frequency at 5.5 GHz. A four-dimensional antenna with a rectangular slot between radiators results in a good impedance matching and a parasitic structure that stands for high isolation performance. The simulation of the antenna is performed on Ansoft High-Frequency Structure Simulator, i.e., HFSS tool which uses a finite element technique that verifies the performance of the proposed antenna and is fully compatible with the developed antenna model measurements. The process of this MIMO antenna is ordered as follows. Section 1 discusses the introduction related to the different MIMO antennas and their performance. In Section 2, the design process for quad-port antenna, i.e., MIMO configuration, is elaborated. The performance of the quad element MIMO antenna and the analysis are described in Section 3. The diversity performance parameter is discussed in Section 4. The experimental validation of the implemented MIMO antenna is discussed in Section 5. A comparison of the implemented MIMO antenna with similar techniques is given in Section 6. Section 7 ultimately concludes the paper.

2. CONFIGURATION OF THE QUAD-PORT ANTENNA

The structure of the implemented quadport antenna is presented in this section. The parameters of the single pentagon radiating element are determined by using Equations (1) and (2), respectively. A typical pentagon has an identical side length shown in Fig. 1. The side lengths of the pentagon can be estimated using Eq. (1) [23]. The area of a typical pentagon can be calculated or derived from its side

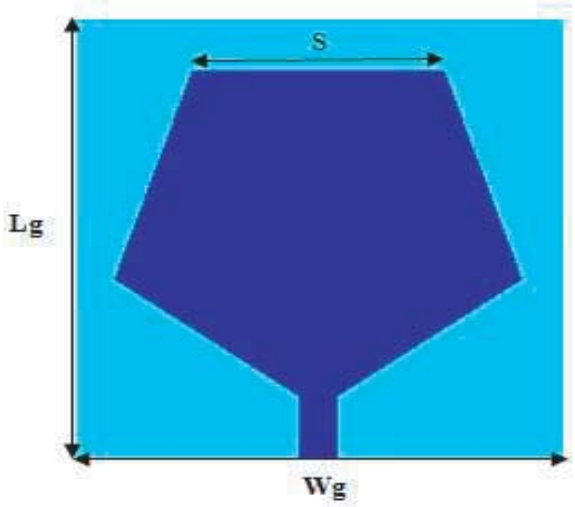

Figure 1. Geometry of the pentagon radiating element.

length (S). Given from the side edges, area (A) of standard pentagon radiating element of the antenna can be estimated using Eq. (2) [23], where 'c' represents the speed of free space of electromagnetic waves, 'f_r' the resonating frequency or operating frequency, 'ε_r' the relative dielectric constant of the substrate material, n the number of sides of the radiating element (for pentagon $n = 5$), and the side length of the regular pentagon is represented as 'S'. '$\varepsilon_{\text{reff}}$' is the effective dielectric constant which is calculated by Eq. (3), where h represents the height of the dielectric substrate. 'L_g' represents the length of the ground plane, and 'W_g' represents the width of the ground plane calculated by Eqs. (4) and (5), respectively [24].

$$S = \frac{2c}{nfr\sqrt{\varepsilon r}} \tag{1}$$

$$A = \frac{S^2 n}{4\tan\left(\frac{180^\circ}{n}\right)} \tag{2}$$

$$\varepsilon_{\text{reff}} = \frac{\varepsilon r + 1}{2}(1 + 0.3h) \tag{3}$$

$$L_g = \frac{0.36c}{fr\sqrt{\varepsilon\text{reff}}} \tag{4}$$

$$W_g = \frac{1.38c}{fr\sqrt{\varepsilon\text{reff}}} \tag{5}$$

As mentioned earlier, the proposed antenna configuration consists of four identical elements. These elements are placed on the same surface, defined as antennas A1, A2, A3, and A4 shown in Fig. 2. As mentioned in the design, each element contains a pentagonal patch and a rectangle combined over the base width, or the base is also called a base rectangle patch. Moreover, rectangle-shaped slots are wisely printed on the pentagonal patch of each element. Each of the components is mounted

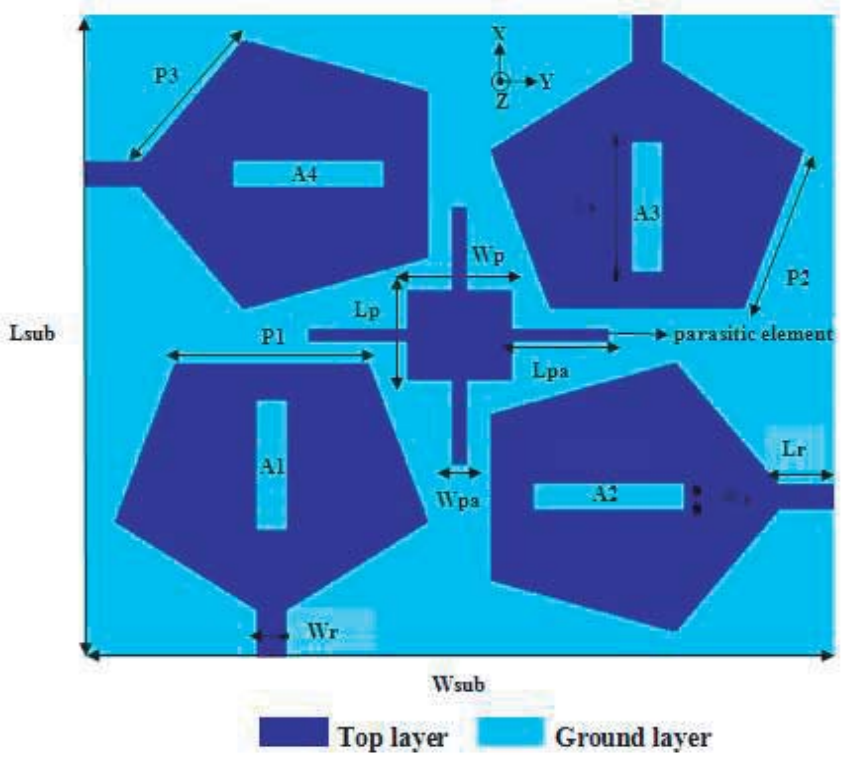

Figure 2. Configuration of the quad element MIMO antenna.

and makes a compact size of 25 mm × 25 mm × 1.6 mm resulting in a MIMO antenna size of only 50 mm × 50 mm × 1.6 mm. The antenna is configured into the FR4 substrate material with a dielectric constant of 4.4 and loss tangent of 0.02. To improve the isolation of the antenna, on the surface of the dielectric substrate a single plus-shaped parasitic structure is uniformly inserted between the antenna elements.

Detailed estimates of the proposed structure are presented in Fig. 2 with optimized parameter values as $L_{sub} = 50$ mm, $W_{sub} = 50$ mm, $P1 = 12.9$ mm, $P2 = 12.9$ mm, $P3 = 11.7$ mm, $L_p = 7$ mm, $W_p = 7$ mm, $L_{pa} = 3$ mm, $W_{pa} = 1$ mm, $L_s = 10$ mm, $W_s = 2$ mm, $L_r = 3.7$ mm, $W_r = 2$ mm.

3. ANALYSIS OF THE QUAD-PORT ANTENNA WITH GEOMETRIC PARAMETER

This section investigates the impacts of the patch slot, parasitic structure, and a base rectangle patch on the overall performance of the implemented quadport MIMO antenna that is discussed in detail.

3.1. Effect of a Rectangular Slot on Patch

As a separate parameter, the results with and without the patch slots are plotted in the section shown in Fig. 4. Based on the outcomes shown in Fig. 4, it is assumed that without the holding patch slot, no notch frequency and better isolation are found. The Wi-MAX frequency band is completely notched limited as of the 5.1–5.8 GHz frequency range. Also, the high isolation performance is achieved through the Wi-MAX frequency band by holding a patch slot. To further examine the impact of the patch slot on antenna execution, a parametric report is performed. It is clarified that the received notch is viewed by slot installation, and therefore it is expected that antenna execution may change if the size of the slots varies. As clearly shown in Fig. 2, the length of the rectangular slot is (L_s) on the radiating patch.

Figure 3(a) shows the configuration of the implemented MIMO antenna without a rectangular patch slot, and Fig. 3(b) shows that with a rectangular patch slot. Fig. 5 shows the effect of changing the L_s value on the return loss (S_{11}) curve. Three values are selected as sample values for this parameter. The results clearly show that as the number of transitions varies from 8 mm to 10 mm in 1 mm step, the limited band turns toward the lower frequency. By studying the notched band operation, it can be seen that at slot length $L_s = 10$ mm, the Wi-MAX band is usually completely suspended by the proposed quad element MIMO antenna. Also, the width of the rectangular slot (W_s) affects the performance of the return loss antenna parameter. The results obtained in Fig. 6 point out that this parameter has a significant impact on return loss (S_{11}) antenna performance. As can be seen, a band-notched frequency at 5.5 GHz is produced at the width of a rectangular slot range of more than 1 mm. At $W_s = 2$ mm slot width, the Wi-MAX band is finally suspended by the implemented MIMO antenna.

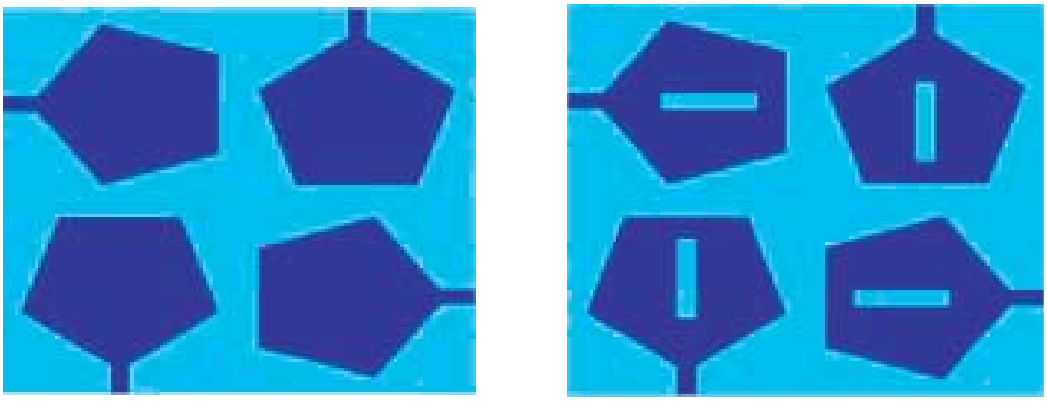

(a) (b)

Figure 3. Configuration of the quad-port MIMO antenna. (a) Without rectangular patch slot. (b) With rectangular patch slot.

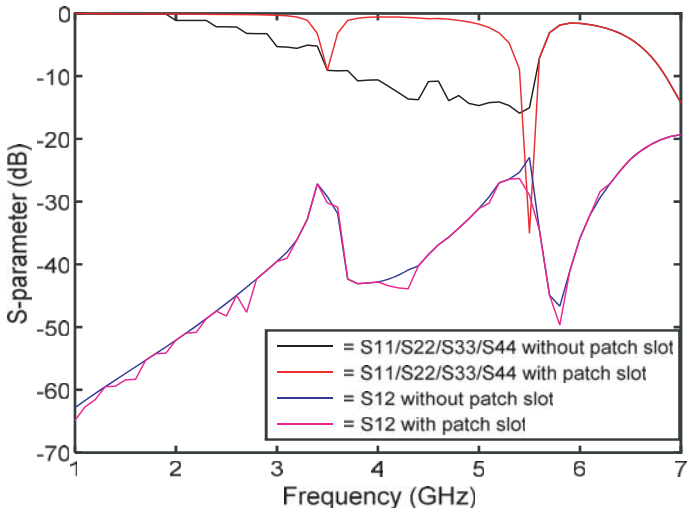

Figure 4. S-parameter curves with and without patch slot.

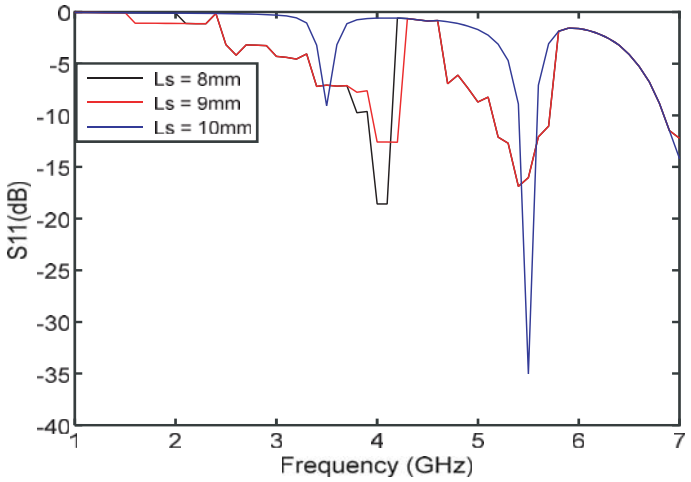

Figure 5. Effect on S_{11} parameter by varying L_s value.

3.2. Effect of the Plus-Shaped Parasitic Element

As mentioned earlier, the plus-shaped parasitic structures are located above the center of the substrate to enhance the separation between the four antenna elements which means isolation present in the proposed MIMO antenna. The parasitic element is not actually connected to the antenna elements presented in the MIMO antenna design. These elements are used in the antenna structure to eliminate part of the interconnected fields between them by forming a reverse field and reducing the total unwanted coupling to the target antenna [25].

To illuminate the effect of the parasitic element, the quad element MIMO designs with and without parasitic elements are performed using the HFSS tool. The curves for S_{12}, S_{13}, and S_{14} are plotted in Fig. 7. It is seen that the highest degree of separation is due to the presence of the plus-shaped parasitic structure. Also, it is quite evident that with the installation of the parasitic element, in the resonance region (around 5.5 GHz), the isolation is 28 dB and again across the band, and it is better than 20 dB of the entire spectrum. This assumption is a direct result of the coupling between the inserted part of the parasitic and other contributing factors in the antenna geometry. As can be seen, when a notched band is at 5.5 GHz, the maximum separation is produced in the width of (W_{pa}) the four-arms of a plus-shaped structure less than 2 mm. In the range of $W_{pa} = 1$ mm width of arms, the maximum

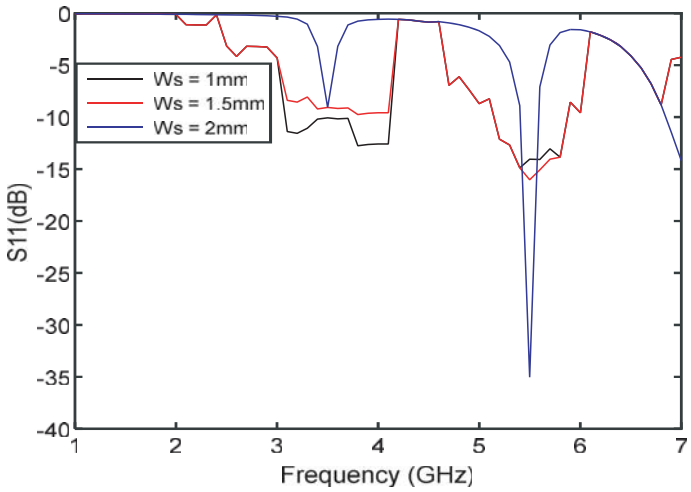

Figure 6. Effect on S_{11} parameter by varying W_s value.

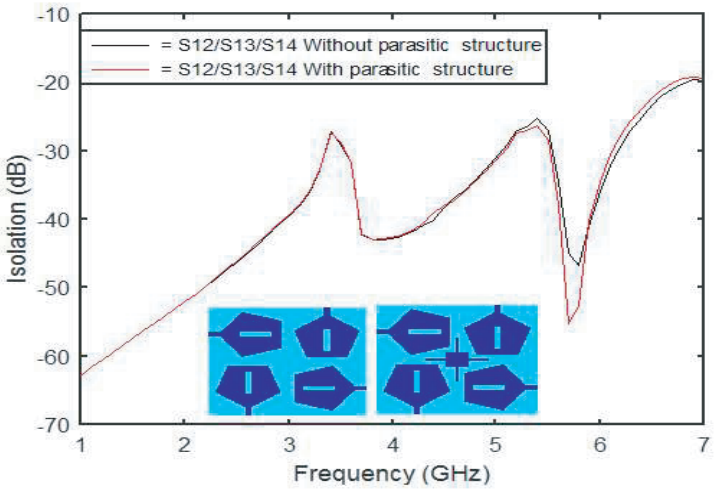

Figure 7. Isolation with and without a parasitic element.

isolation performance of the Wi-MAX is achieved by the proposed MIMO antenna, and and the results are plotted in Fig. 8.

3.3. Effect of a Base Rectangle Patch

The alignment of the used MIMO antenna with and without the base rectangle patch is shown in Fig. 9. It is assumed that the base of the rectangle is connected to the patch, and other than holding such a geometry, no notch frequency is found at 5.5 GHz. The length of the base rectangle patch is (L_r), and the width is (W_r). The Wi-MAX frequency band is completely limited to the frequency range of 5.1–5.8 GHz using a base rectangle radiator device. Also, the high impedance performance of the simulations is achieved with the band-frequency of Wi-MAX by holding the geometry. To further evaluate the impact of the input of the base rectangle patch antenna, a parametric report is shown. It is pointed out that the 5.5 GHz notch is viewed by the installation of a base rectangle patch where without using the base rectangle patch the notch is available at 3.7 GHz and 5.6 GHz with very low bandwidth performance from 5.4 to 5.7 GHz, so it is expected that the antenna execution may change if the size of the width (W_r) of the base rectangle patch varies. Frequencies converge on the right side of the notch fine point required with poor disturbance performance.

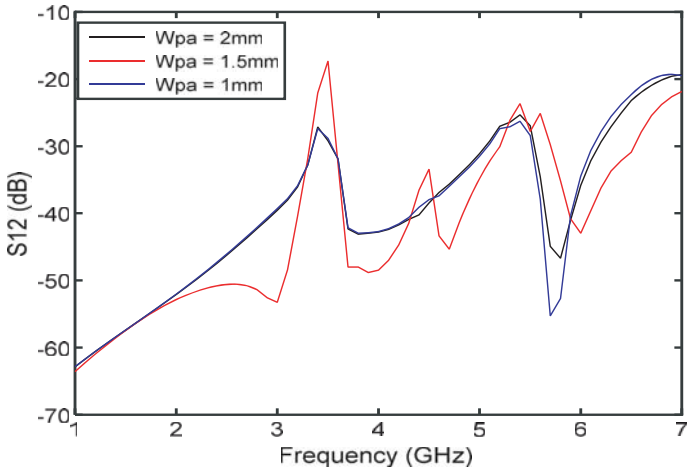

Figure 8. Effect on S_{12} parameter by varying W_{pa} value.

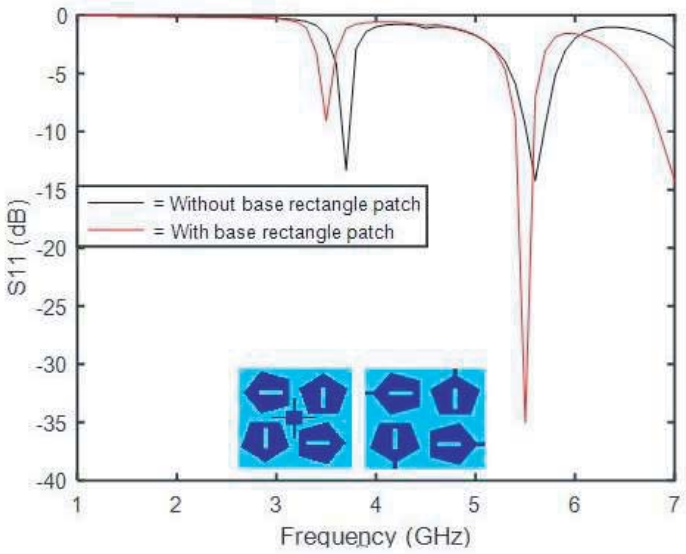

Figure 9. Effect on S_{11} parameter with and without base rectangle patch.

4. PERFORMANCE CHARACTERISTICS OF THE QUAD-PORT ANTENNA

In this section, the variability or diversity performance of the quad-port antenna is identified where the implemented antenna can be analyzed for how well it has performed in a diverse environment. The different parameters such as Diversity Gain (DG), Mean Effective Gain (MEG) and Total Active Reflection Coefficient (TARC). These parameters are important for better visualization of the MIMO antenna system because the scatter matrix alone is not sufficient to demonstrate the efficiency and bandwidth performance of the MIMO antenna system [26].

4.1. Diversity Gain (DG)

The following parameter for the study is the diversity gain, also an important diversity performance parameter. This parameter is denoted by DG and is defined as in Eq. (6) [27]. Eq. (6) represents that the diversity gain dependent on the ECC parameter.

The diversity gain of an antenna is a function of Envelope Correlation Coefficient (ECC). The parameter ECC depends upon the mutual coupling between antenna ports. Therefore, improvement

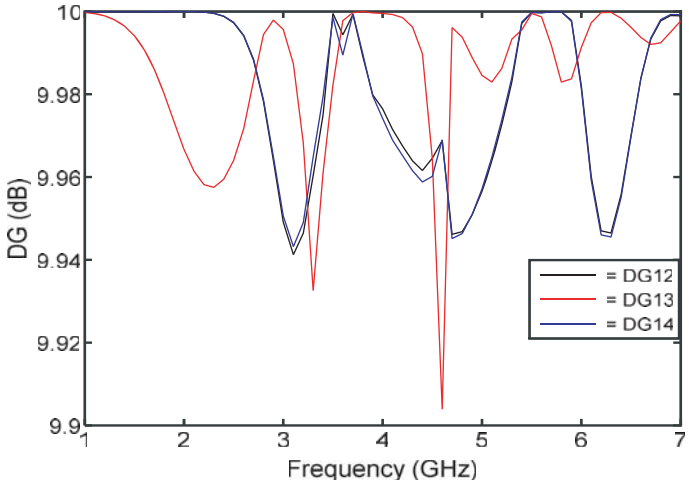

Figure 10. DG parameter of the MIMO antenna.

in the mutual coupling between antenna ports leads to increase in diversity gain (DG) of an antenna. The resulting diversity gain is shown in Fig. 10. This shows values above 9.99 dB across the Wi-Max frequency band range. The value of DG_{12} is 9.992 dB; DG_{13} is 9.991 dB; and DG_{14} is 9.994 dB, found to satisfy the proposed MIMO application requirements. ij is the transfer signal from port j to port i.

$$\mathrm{DG}_{(ij)} = 10\sqrt{1-\mathrm{ECC}^2_{(ij)}} \tag{6}$$

4.2. Total Active Reflection Coefficient (TARC)

Taking into account the constructive and destructive interactive signals in each antenna signal combination, total active reflection coefficient values [28] are also investigated. TARC is the sum of the square root of the combined energy or total rejected power divided by the square root of the total incident energy or power of the MIMO antenna. TARC also defines the operating or active band and radiation characteristics mechanism of a MIMO antenna in which all stages of the input signal are different.

$$\mathrm{TARC}_{(ij)} = \sqrt{\frac{|Sii + Sij|^2 + |Sji + Sjj|^2}{2}} \tag{7}$$

where Sii is the active signal from port i to port i, and Sji is the transfer signal from port i to port j. The same definitions are used in Sjj and Sij, and the only difference is in the exit port order. The TARC is represented in terms of a 2-port of the MIMO antenna as in Eq. (7) [29]. The value of TARC_{12} is -18 dB; TARC_{13} is -17 dB; and TARC_{14} is -14 dB. In Fig. 11, it is observed that the TARC across the Wi-Max frequency band range is less than -14 dB.

4.3. Mean Effective Gain (MEG)

The mean effective gain (MEG) values of the implemented Wi-MAX antennas are calculated using the scattering parametric distribution method [30]. It is observed that antennas have good MEG values which occur primarily due to better separation between MIMO antenna elements in Fig. 12.

$$\mathrm{MEG}_{(i)} = 0.5\left[1 - \sum_{j=1}^{M} |Sij|^2\right] \tag{8}$$

Also, the MEG ratio of the various ports is approximately equal to 1, and for this design, MEG is 0.912 dB which ensures the best performance of the variants of the MIMO system. MEG_1 is -3.107 dB; MEG_2 is -3.120 dB; MEG_3 is -3.096 dB; and MEG_4 is -3.089 dB. In practical applications, less than

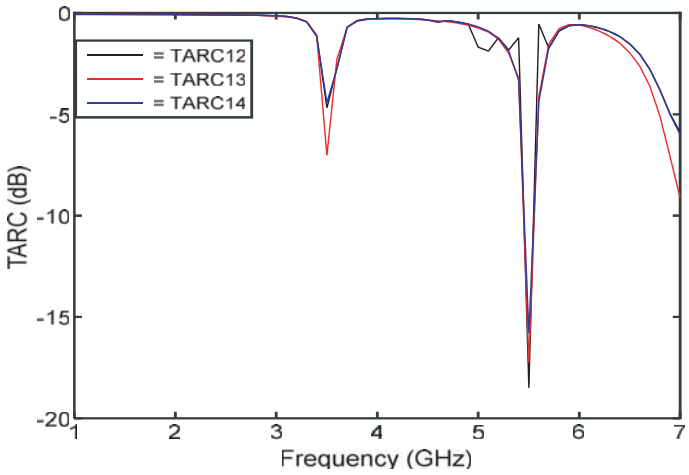

Figure 11. TARC parameter of the MIMO antenna.

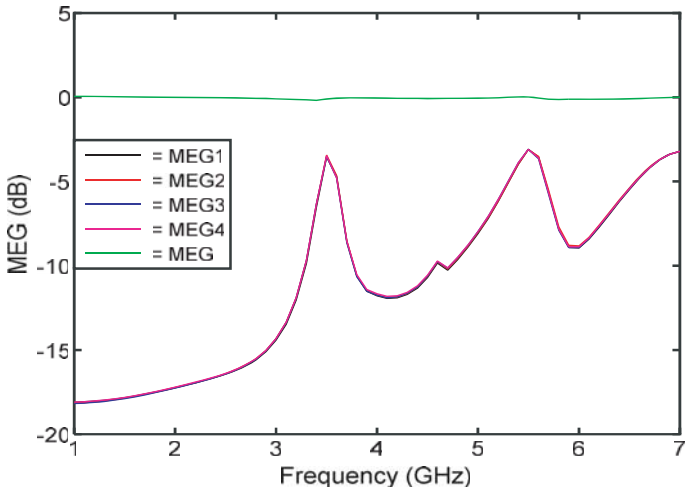

Figure 12. MEG parameter of the MIMO antenna.

3 dB, MEG is considered an appropriate performance. The MEG is represented in terms of a scattering parameter in Eq. (8), where Sij is the transfer signal from port j to port i, and M is the number of iterations which depends on the number of ports.

5. EXPERIMENTAL VALIDATION OF THE QUAD-PORT ANTENNA

This section establishes a platform for evaluating prototype measurement and comparison results. The fabricated antenna structure is shown in Fig. 13. A top view of the fabricated antenna is shown in Fig. 13(a), rear view shown in Fig. 13(b), and prototype outcome on Rohde-Schwartz VNA ZVL13 shown in Fig. 13(c).

It should be noted that the antenna parameter estimation is performed by a Rohde-Schwartz Vector Network Analyzer ZVL13 at the antenna and microwave laboratory.

5.1. S-Parameter

The simulated and measured return loss parameters (S_{11}, S_{22}, S_{33}, S_{44}) are shown in Fig. 14 for comparison. Fig. 14 shows that the antenna has the simulated impedance bandwidth at $S_{11} \leq -10$ dB in notch-band from 5.1 GHz to 5.8 GHz with isolation according to S_{12} better than 28 dB at the same

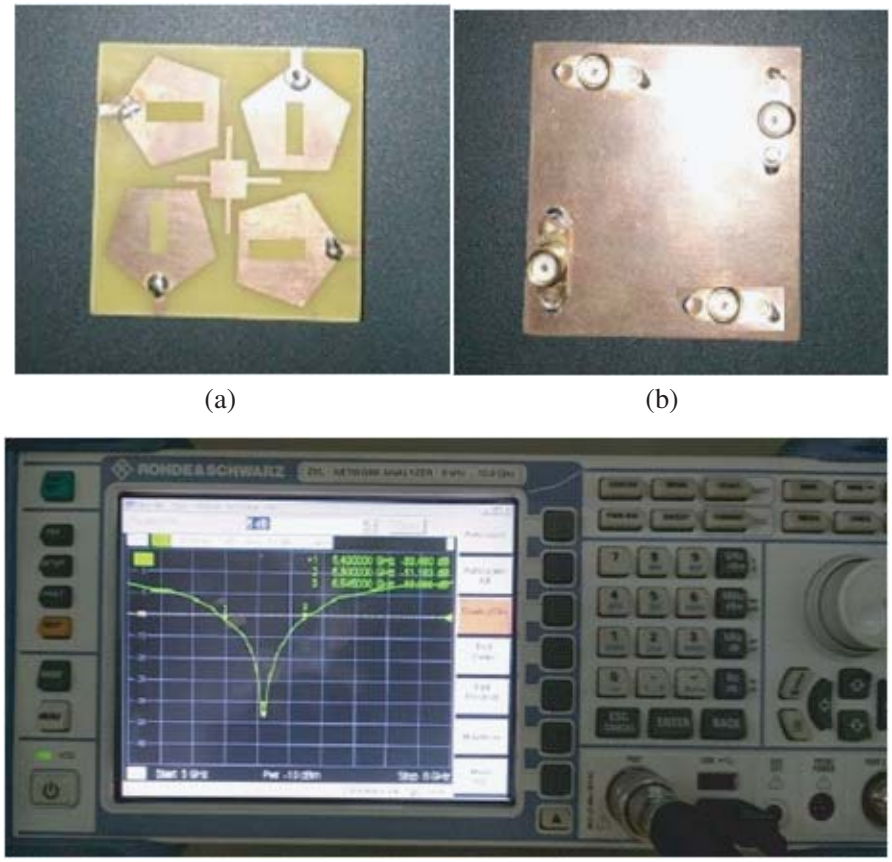

Figure 13. Fabricated structure of proposed MIMO antenna. (a) Top view. (b) Rear view. (c) Prototype outcome on Rohde-Schwartz VNA ZVL13.

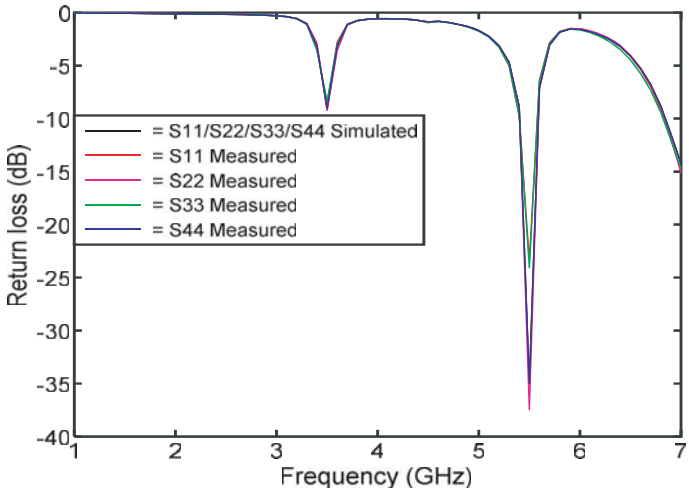

Figure 14. Calibration of the simulated and measured return loss.

frequency range (5.1 to 5.8 GHz). This indicates that the antenna is suitable for MIMO operation throughout the Wi-MAX band application. There are some differences between the simulated and measured return losses (S_{11}, S_{22}, S_{33}, and S_{44}) and the isolation (S_{12}) parameter.

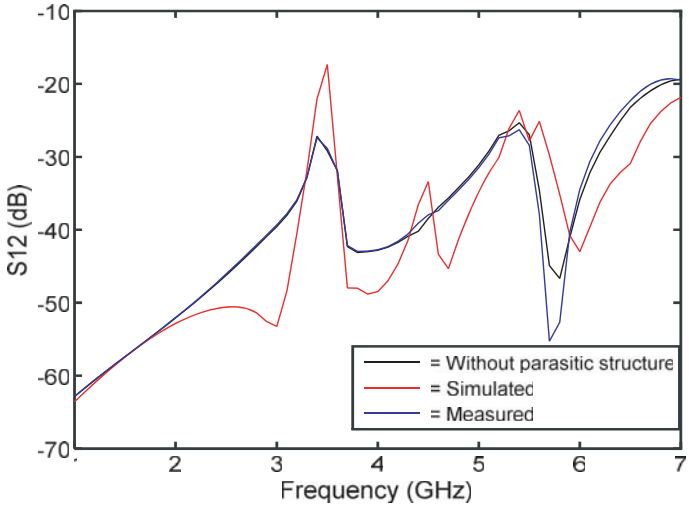

Figure 15. Calibration of the simulated and measured S_{12}.

For example, Fig. 14 shows that the band in measured outcomes is slightly restricted compared to the simulated one which means that the return loss ($S_{11}/S_{22}/S_{33}/S_{44}$) is -37 dB in band 5.2 to 5.8 GHz, and Fig. 15 shows that at the notch band frequency 5.5 GHz isolation (S_{12}) between the antenna elements is 32 dB, and this parameter is an important parameter in MIMO system because the energy of one antenna is coupled with other antenna elements due to which overall radiation performance of the antenna decreases, which shows that isolation capability is higher than the simulated result. As can be seen from the measured result, the proposed antenna resonates considerably well in the operating bands of 5.2 to 5.8 GHz with notched frequency at 5.5 GHz. However, some differences are observed due to compression tolerances, fabrication errors, and losses because of the connectors.

5.2. Gain and Radiation Efficiency

The implemented MIMO antenna system contains band-notched features. Therefore, in order to have a good Wi-MAX band analysis, the peak gain (PG) and radiation efficiency (RE) of the proposed system are calculated. Generally, it is desirable to obtain low gain and high efficiency at notching frequencies. This peak gain parameter is defined in the far-field region of the antenna. The radiation efficiency and peak gain of measured and simulated of the proposed antenna are shown in Fig. 16 and Fig. 17.

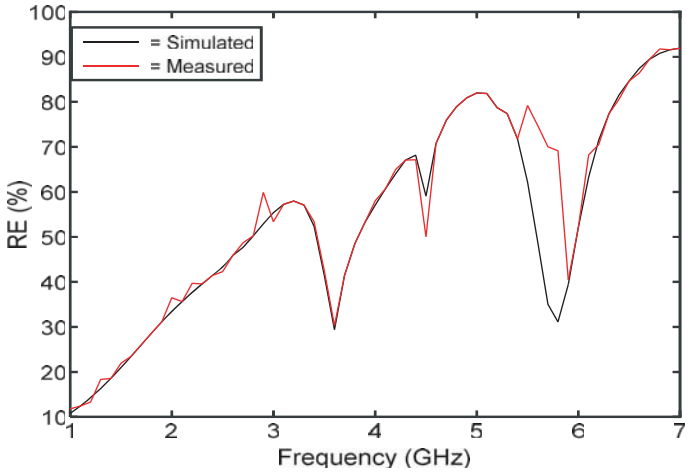

Figure 16. Calibration of the simulated and measured radiation efficiency.

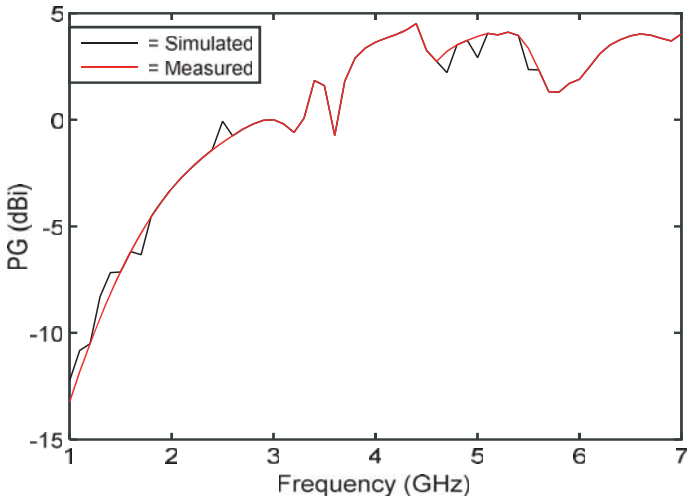

Figure 17. Calibration of the simulated and measured peak gain.

At higher frequencies, Fig. 16 shows that the measured efficiency corresponds well to the simulated result. However, at low frequencies, the measured efficiency is much lower than the simulated one, which is caused by the feeding cable used in the measurement [31]. The measured and simulated radiation efficiencies agree very well for the Wi-MAX band application. The performance of the antenna in terms of radiation efficiency in the Wi-MAX band is better than 70%, and at the notched frequency, it is 79% at 5.5 GHz. Fig. 17 shows that in the notched band, the peak gain varies from 2.9 to 1.9 dBi, and for the notched frequency it is 3.1 dBi. It is also observed that the measured results are smaller than the simulated output due to the effects of the feed network and the power loss of the original antenna material. It clearly shows that the proposed antenna offers good values for gain and efficient response across the Wi-MAX band and in the inaccessible Wi-MAX band also for maximum efficiency and gain.

5.3. Envelope Correlation Coefficient (ECC)

The investigation of the Envelope Correlation Coefficient can help to verify the effectiveness of the MIMO system. The ECC parameter specifies how antenna objects are separated or isolated. It can be calculated in the two ways first from the use of pattern dependence on field radiation and the other from scattering-parameters. The interaction between the antenna elements is indicated by ECC and calculated by the scattering parameters as reported in Eq. (9) [27], where Sii is the active signal from

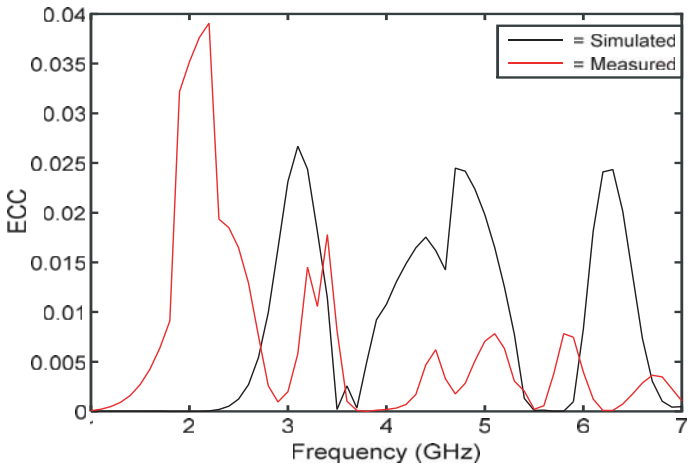

Figure 18. Calibration of the simulated and measured ECC.

port i to port i also called return loss parameter, and Sji is the transfer signal from port i to port j also called isolation parameter.

$$\mathrm{ECC}_{(ij)}=\frac{|S*iiSij+S*jiSjj|}{\left(\left(1-|Sii|^2+|Sji|^2\right)\right)\left(\left(1-|Sjj|^2+|Sij|^2\right)\right)} \tag{9}$$

The same definitions are used in Sjj and Sij, and the only difference is in the exit port order. The '*' represents the complex conjugate term. After obtaining the appropriate scattering -parameters, the generated ECC is measured and simulated in Fig. 18, and the results indicate that the ECC points are less than 0.0006 across the band except that there is a very low value near the corresponding notch band at 5.5 GHz which is 0.000041. Despite this, it still meets the requirement for good diversity performance of the antenna that ECC in the bandwidth should be less than 0.5. It can be concluded that the correlation coefficient of the four antenna elements is very low, which is why the features of the proposed MIMO antenna are applicable to wireless applications with good diversity results.

6. COMPARISON WITH OTHER PREVIOUS SIMILAR ANTENNA DESIGNS

To exhibit the benefits of the implemented design over the same general previous designs, comparisons are made in Table 1. Comparative names contain the number of elements in MIMO antennas, bandwidth, size, notched-band, and itself. Details are summarized in Table 1 which points out that the antenna proposed in this work is the smallest when considering the number of elements presented in MIMO antennas with other designs. However, better isolation is not obtained regarding the antenna structure in [13, 14, 16–18]. Also, the structures proposed in [16, 17], though having a small size and different base (substrate) element compared to only with two antenna elements, still offer less isolation between the MIMO antenna elements. These comparisons bring the proposed structure over other similarities and satisfy the need for a Wi-MAX band that is not included with high isolation in other designs.

Table 1. Comparison of the proposed antenna with other previous similar antennas.

Ref.	No. of elements	Size of the antenna (mm^3)	Substrate material	Notch band (GHz)	Bandwidth (GHz)	Isolation (dB)
[11]	2	$43 \times 20 \times 0.762$	Neltec	5.5	3.1–10.6	< 20
[13]	2	$40 \times 25 \times 1.6$	FR4	5.5	3.3–10.8	< 15
[14]	4	$45 \times 45 \times 1.6$	FR4	5.5	2–10.6	< 17
[15]	2	$23 \times 39.8 \times 1.524$	Rogers TMM4	5.5	2–12	< 20
[16]	2	$38.5 \times 38.5 \times 1.6$	FR4	5.5	3.08–11.8	< 15
[17]	2	$22 \times 29 \times 0.8$	RO4003	5.5	3–10.6	< 17
[18]	4	$39.8 \times 50 \times 1.524$	Rogers TMM4	5.5	2.7–12	< 17
[20]	2	$30 \times 30 \times 0.8$	FR4	5.5	3.08–10.98	< 20
PW	4	$50 \times 50 \times 1.6$	FR4	5.5	5.1–5.8	< 32

7. CONCLUSION

The wide range and integrated dimensions of $50 \times 50\,mm^2$ MIMO antennas are designed and analyzed with a Wi-MAX notched portable application. The simplest and least expensive design of the proposed MIMO antenna is composed of four monopole antennas. Each monopole has a pentagonal patch with rectangular slots and a simple ground plane. Rectangle-shaped slots are used to produce the notch band at 5.5 GHz in the Wi-MAX frequency range. Later, to improve the MIMO antenna element separation, a single plus-shaped parasitic structure is uniformly inserted between the antenna elements to diminish the mutual coupling effect between the elements below 32 dB. It is shown that the operating range

obtained by $|S_{11}| \leq -15\,\text{dB}$ of the proposed antenna covers the 5.1 to 5.8 GHz range and the band notched frequency at 5.5 GHz. Also gain, efficiency, and ECC are calculated for the notched frequency as 3.1 dBi, 79%, and 0.000041, respectively. Alternatively, a close agreement is found between the simulated and measured results containing the proposed MIMO antenna as the one suitable for wireless Wi-MAX band applications.

REFERENCES

1. Cheng, C.-M., et al., "Four antennas on smart watch for GPS/UMTS/ WLAN MIMO application," *IEEE Intl. Conf. on Comp. Electromagn. (ICCEM)*, Vol. 2017, 346–348, IEEE, Kumamoto, Japan, 2017.
2. Li, Q., et al., "MIMO techniques in WiMAX and LTE: A feature overview," *IEEE Commun. Mag.*, Vol. 48, No. 5, 8692, 2010.
3. Azarm, B., Ch. Ghobadi, et al., "A compact WiMAX band-notched UWB MIMO antenna with high isolation," *Radioengineering*, Vol. 27, No. 4, 983989, 2018.
4. Quddus, A., et al., "Compact electronically reconfigurable WiMAX band-notched ultra-wideband MIMO ntenna," *Radioengineering*, Vol. 27, No. 4, 9981005, 2018.
5. Kamonsin, W., et al., "Dual-band metamaterial based on Jerusalem cross structure with interdigital technique for LTE and WLAN systems," *IEEE Access*, Vol. 8, 2156521572, 2020.
6. Brown, A. K., et al., "Compact reconfigurable multiple-input-multiple-output antenna for ultra wideband applications," *IET Microw. Antennas Propag.*, Vol. 10, No. 4, 413419, 2016.
7. Liu, L., et al., "Compact MIMO antenna for portable UWB applications with band-notched characteristic," *IEEE Trans. Antennas Propagat.*, Vol. 63, No. 5, 1917–1924, 2015.
8. Dissanayake, T. and K. P. Esselle, "Prediction of the Notch frequency of slot loaded printed UWB antennas," *IEEE Trans. Antennas Propagat.*, Vol. 55, No. 11, 33203325, 2007.
9. Turitsyna, E. G. and S. Webb, "Simple design of FBG-based VSB filters for ultra-dense WDM transmission," *Electron. Lett.*, Vol. 41, No. 2, 89, 2005.
10. Ojaroudi, M., et al., "Dual band-notched small monopole antenna with novel W-shaped conductor backed-plane and novel T-shaped slot for UWB applications," *IET Microw. Antennas Propag.*, Vol. 7, No. 1, 814, 2013.
11. Sipal, D., et al., "Compact band-notched UWB antenna for MIMO applications in portable wireless devices," *Microw. Opt. Technol. Lett.*, Vol. 58, No. 6, 1390–1394, 2016.
12. Kang, L., et al., "Miniaturized band-notched UWB MIMO antenna with high isolation," *Microw. Opt. Technol. Lett.*, Vol. 58, No. 4, 878–881, 2016.
13. Tripathi, S., et al., "A compact octagonal fractal UWB MIMO antenna with WLAN band-rejection," *Microw. Opt. Technol. Lett.*, Vol. 57, No. 8, 1919–1925, 2015.
14. Tripathi, S., et al., "A compact Koch fractal UWB MIMO antenna with WLAN band-rejection," *Antennas Wirel. Propag. Lett.*, Vol. 14, 1565–1568, 2015.
15. Naqvi, A., et al., "Compact planar UWB MIMO antenna with on-demand WLAN rejection," *Electron. Lett.*, Vol. 51, No. 13, 963–964, 2015.
16. Kang, L., et al., "Compact offset microstrip-Fed MIMO antenna for band-notched UWB applications," *Antennas Wirel. Propag. Lett.*, Vol. 14, 1754–1757, 2015.
17. Malekpour, N., et al., "Compact UWB MIMO antenna with band-notched characteristic," *Microw. Opt. Technol. Lett.*, Vol. 59, No. 5, 1037–1041, 2017.
18. Khan, S. M., et al., "A compact four elements UWB MIMO antenna with on-demand WLAN rejection," *Microw. Opt. Technol. Lett.*, Vol. 58, No. 2, 270–276, 2016.
19. Huang, H.-F. and S.-G. Xiao, "Mimo antenna with high frequency selectivity and controllable bandwidth for band-notched UWB applications," *Microw. Opt. Technol. Lett.*, Vol. 58, No. 8, 1886–1891, 2016.
20. Biswal, S. P. and S. Das, "A low-profile dual port UWB-MIMO/diversity antenna with band rejection ability," *Int. J. RF Microw. Comput. Aid. Eng.*, Vol. 28, No. 1, e21159, 2018.

21. Srivastava, G. and B. K. Kanuijia, "Compact dual band-notched UWB MIMO antenna with shared radiator," *Microw. Opt. Technol. Lett.*, Vol. 57, No. 12, 2886–2891, 2015.
22. Huang, H., et al., "Compact polarization diversity ultrawideband MIMO antenna with triple band-notched characteristics," *Microw. Opt. Technol. Lett.*, Vol. 57, No. 4, 946–953, 2015.
23. Bhadade, R. S. and S. P. Mahajan, "High gain circularly polarized pentagonal microstrip for massive MIMO base station,",*AEM*, Vol. 8, No. 3, 83–91, 2019.
24. Viraja, B., et al., *Design and Implementation of Pentagon Patch Antennas WithSlit for Multiband Wireless Applications Ls = 14431448*, 2018.
25. Christina, A., J. Malathi, and D. Thiripurasundari, "Review on isolation techniques in MIMO antenna systems," *Indian J. Sci. Technol.*, Vol. 9, No. 35, 2016.
26. Chae, S. H., et al., "Analysis of mutualcoupling, correlations, and TARC in WiBro MIMO array antenna," *Antennas Wirel. Propag. Lett.*, Vol. 6, 122–125, 2007.
27. Ibrahim, A. A. and M. A. Abdalla, "CRLH MIMO antenna with reversal configuration," *AEU Int. J. Electron. Commun.*, Vol. 70, No. 9, 1134–1141, 2016.
28. Browne, D. W., et al., "Experiments with compact antenna arrays for MIMO radio communications," *IEEE Trans. Antennas Propagat.*, Vol. 54, No. 11, 3239–3250, 2006.
29. Manteghi, M. and Y. Rahmat-Samii, "Multiport characteristics of a wide-band cavity backed annular patch antenna for multipolarization operations," *IEEE Trans. Antennas Propagat.*, Vol. 53, No. 1, 466–474, 2005.
30. Nasir, J., et al., "Throughput measurement of a dual-band MIMO rectangular dielectric resonator antenna for LTE applications," *Sensors*, Vol. 17, No. 1, 148, 2017.
31. Liu, L., et al., "Cable effects on measuring small planar UWB monopole antennas ultrawideband — Curr," *Status Futur Trends*, 2012.